Peer-reviewed version available at *Metals* **2020**, *10*, 1057; doi:10.3390/met10081057

Article

On the adsorption of cerium(III) using multiwalled carbon nanotubes

Francisco J. Alguacil, Irene García-Díaz, Esther Escudero Baquero, Olga Rodríguez Largo, Félix A. López*

Centro Nacional de Investigaciones Metalurgicas (CSIC). Avda. Gregorio del Amo 8. 28040 Madrid. Spain.
* Correspondence: f.lopez@csic.es; Tel.: +34-915538900 (F.L.)

Abstract: Commercially available oxidized (carboxylic groups) and non-oxidized multiwalled carbon nanotubes were studied as adsorbents of cerium(III) in batch operation mode. Several variables affecting the rare earth adsorption were investigated, including: the stirring speed applied to the system, the pH of the solution and the metal concentration and carbon dosages. Although the removal of cerium from the solution is different and dependent upon the adsorbent type: i) adsorption in non-oxidized multiwalled carbon nanotubes, ii) cation exchange in the case of using oxidized multiwalled carbon nanotubes, the adsorption kinetics, the rate law and the isotherm models are the same for both adsorbents: pseudo-second order, film diffusion and Langmuir Type-1, respectively. Cerium is desorbed from loaded adsorbents using acidic solutions.

Keywords: adsorption; carbon nanotubes; rare earth

---

1. Introduction

In comparison with other separation technologies, adsorption is one of the most used due to its operational characteristics and the possibility of its uses in dilute solutions and even non-clarified ones [1]. Thus, from long time ago adsorbents, of various nature, are used as medium to remove both valuable and non-valuable, including hazardous, metals or solutes from aqueous solutions[2,3]. Including in these adsorbents, carbon nanotubes in various configurations are considered of a particular interest in this task [4–7].

One of these applications is in the case of the recovery of rare earths from various aqueous solutions [8,9]. Nowadays, with a global mine production of 210000 ton in 2019 [10], the recovery of these rare earths is of a particular interest due to their use in smart technologies and scarce availability of their resources (i.e. here in the European Union), thus, the recycling of these metals became of interest. However, in the European Union the rate of their recyclability is around 6% and 7% for the heavy and light rare earths, respectively [11,12].

Cerium and cerium compounds are of a particular importance due to their application in strategical sectors, including metal alloys, glass, adsorbent, catalysts, biomedical applications [13–20], and also in a growing sector such as rechargeable batteries [21–23], thus, cerium is considered a critical raw material by the EU [24].

Recent investigations on the adsorption of cerium(III) showed that a variety of adsorbents are useful for this task, i.e, K10-montmorillonite removes Ce(III) from solutions via a cation exchange mechanism [25], whereas simulated radioactive Ce(III) can be removed from solutions using magnetic trioctylamine-polystyrene composite microspheres [26]. Nitrolite is used as adsorbent for a series of light rare earths and Cr(III) [27], in all the cases, the adsorption increases with the increase of the pH (up to pH 9), however, metal precipitation phenomena occurs together with a true adsorption process. Others adsorbents recently used for the removal of cerium(III), from aqueous solutions, are various soils [28], montmorillonite nanoclay [29], HKUST-1 framework [30] and cherty rocks [31], in this work, and being one of the rare exception in adsorption experiments, the stirring speed applied to the system is considered; also, and relying in not a true adsorption process but in an ion exchange process, several ion exchangers, namely Amberlite 200C Na, Amberlite 200C, Dowex

Peer-reviewed version available at Metals 2020, 10, 1057; doi:10.3390/met10081057

M4195 and Diphonix resins, are used to investigate the recovery of Ce(III) (among other metals)) from acidic solutions [32,33].

The present investigation shows and experimental work on the adsorption of cerium(III), from aqueous solutions, using two carbon nanomaterials: non-oxidized multiwalled carbon nanotubes (MWCNTs) and oxidized multiwalled carbon nanotubes (ox-MWCNTs), in this case, the material has been functionalized by carboxylic acid groups. Several experimental variables affecting cerium(III) adsorption were investigated, and the data were fitted to several models to explain the kinetics, rate law and adsorption isotherms associated with this adsorption. Metal-loaded onto both nanomaterials can be desorbed by the use of acidic solutions..

2. Materials and Methods

The adsorbents were used as supplied by the vendor (Sigma-Aldrich), in the case of the oxidized material, carboxylic acid was the active group. Main characteristics of the both adsorbents were given elsewhere [4,34]. On both carbonaceous nanomaterials, Z potential was measured using a Zetasizer Malvern Nano ZS at 25º C. Aqueous suspensions were prepared in the 1-13 pH range, and using HCl and NaOH solutions to control the pH value. The concentration of the carbon material was adjusted to a value of 0.1 g/L. The suspensions were dispersed with a Bandelin Electronic Sonopuls HD 3100 sonicator, using an amplitude of 60% for 150 s.

Other chemicals used were of AR grade. Cerium(III) solutions were prepared by dissolving $Ce(NO_3)_3·6H_2O$ in distilled water, and the different concentrations used in the experiments were prepared from this stock solution. The pH values of the aqueous solutions were adjusted by addition of nitric acid. During the experiments, the pH was continuously monitorized using a 605 pH-meter (Crison).

The adsorption experiments were carried out in a glass vessel provided of mechanical stirring. Cerium concentrations in the aqueous solution were analyzed by ICP-OES (Agilent Technologies 5100), with an associated analytical error of ±3%. The percentage of cerium remaining in the aqueous solution was determined by the next relationship:

$$\% = \frac{[\mathrm{Ce}]_{\mathrm{aq,t}}}{[\mathrm{Ce}]_{\mathrm{aq,o}}} \times 100 \tag{1}$$

where $[Ce]_{aq,0}$ and $[Ce]_{aq,t}$ were the initial and at an elapsed time cerium concentrations in the solution, respectively. Cerium concentrations in the adsorbents were calculated by the mass balance.

Desorption experiments were performed in the same basis as above.

3. Results

Measurement of Z potential values on MWCNTs and ox-MWCNTs, at different pH values, showed that the isoelectronic points (IEP) are 1.22 and 0.26 for both nanomaterials, respectively. At pH values lower than the pH(IEP), the charge of the adsorbent surface is positive, however, when the pH increases the surface has a negative charge. This change in the surface charge may have, at it is demonstrated latter, a great influence on the adsorption results.

3.1. Adsorption using non-oxidized multiwalled carbon nanotubes (MWCNTs)

The adsorption of cerium(III) by MWCNTs is represented by the general equilibrium:

$$Ce_{aq}^{3+} \leftrightarrow Ce_{c}^{3+} \tag{2}$$

where aq and c denote species in the aqueous and carbon phases, respectively.

3.1.1. Influence of the stirring speed

Peer-reviewed version available at *Metals* **2020**, *10*, 1057; doi:10.3390/met10081057

Experiments to investigate the influence of the stirring speed applied on the system were first investigated by the use of aqueous solutions of 0.01 g/L Ce(III) at pH 6, and carbon dosage of 4 g/L. In these series of experiments, the stirring speed was varied from 500 to 1000 min^{-1}, whereas the temperature was maintained at 25º C. The results were summarized in Table 1.

Table 1. Influence of stirring speed on cerium adsorption.

Stirring speed, min^{-1}	% Ce(III) adsorption
500	99
750	98
1000	96

It can be seen that cerium uptake becomes practically independent of the stirring speed, though a slight decreased in metal uptake can be observed from 500 to 1000 min^{-1}, probably due to the presence of local equilibria produced by the increase of the centrifugal force as the stirring speed increased. These results demonstrated that around 500 min^{-1}, a minimum value of the thickness of the aqueous phase boundary layer was reached.

The experimental results yielded at this stirring speed were used to estimate the kinetic order associated to this system, and the results from this fit resulted in that cerium adsorption by these MWCNTs was best represented by the pseudo-second order kinetic model (r^2= 0.9982)[34]:

$$\frac{t}{[Ce]_{c,t}} = \frac{1}{k[Ce]_{c,e}^2} + \frac{1}{[Ce]_{c,e}}t \tag{3}$$

In the above equation, [Ce]c,t and [Ce]c,e are the cerium concentrations in the carbon at an elapsed time and at equilibrium, respectively, and k is the rate constant associated with the model. The fit indicated that k is estimated as 0.38 g/mg.min, and [Ce]c,e is 2.6 mg/g, which fits very well with the value of 2.5 mg/g experimentally yielded. Since that experimental data fitted to the pseudo-second order model, a chemical activation between MWCNTs and the cerium ions might be possible bay [35].

3.1.2. Influence of aqueous pH

Table 2 shows the results obtained from the adsorption of cerium at different aqueous pH values. The carbon dosage was of 3 g/L. The aqueous solution contained 0.01 g/L Ce(III) at pH values ranging from 1 to 6.

Table 2. Influence of the aqueous pH.

pH	% Ce(III) adsorption
1	1
2	10
3	29
4	78
5	85
6	99

Temperature: 25ºC. Time: 5h. Stirring speed: 500 min^{-1}

The results shown in Table 2 demonstrate that the increase of the aqueous pH increased the percentage of metal uptake onto the adsorbent. These results agreed with the isoelectronic point of

Peer-reviewed version available at Metals 2020, 10, 1057; doi:10.3390/met10081057

this adsorbent (1.22) thus and since the pH increases from this point, the carbon surface becomes negatively charged, and thus, promoting cation uptake.

The results at pH 6 were used to estimate the rate law explaining cerium adsorption onto these nanomaterials. The results from this fit demonstrated that aqueous diffusion controlled such uptake (r^2= 0.9815) [34]:

$$ln(1-F) = -kt \tag{4}$$

where F represented the factorial approach to the equilibrium, defined as:

$$F = \frac{[Ce]_{c,t}}{[Ce]_{c,e}} \tag{5}$$

Accordingly, with eq. (4), the rate constant k for the model was estimated as 0.02 min^{-1}. It is worth to mention here, that in a series of adsorption systems the pseudo-second order kinetic model was associated with an aqueous diffusion model [36].

3.1.3. Effect of the initial metal concentration on cerium uptake

Table 3 shows the variation in the percentage of cerium adsorption against the concentration of cerium ranging from 0.01 to 0.08 g/L in the aqueous solution.

Table 3. Variation in the metal adsorption with the initial cerium concentration.

$[Ce]_{aq,0}$, g/L	% Ce(III) adsorption
0.01	99
0.02	78
0.03	77
0.04	76
0.06	52
0.08	38

Aqueous phase: Ce(III) at pH 6. Carbon dosage: 3 g/L. Temperature: 25º C. Time: 5 h

It can be observed that with the present experimental conditions, the percentage of metal adsorption onto the multiwalled carbon nanotubes tends to decrease. The data derived from Table 3 were used to estimate the isotherm model which best fitted to the adsorption results, the results from this fit indicated that that Langmuir Type-1 isotherm presented the best fit (r2= 0.9987) to these experimental data:

$$\frac{[Ce]_{aq,e}}{[Ce]_{c,t}} = \frac{1}{k[Ce]_{c,m}} + \frac{1}{[Ce]_{c,m}}[Ce]_{aq,e} \tag{6}$$

where $[Ce]_{aq,e}$ represented the metal concentration in the aqueous phase at the equilibrium, and $[Ce]_{c,m}$ to the maximum cerium concentration adsorbed onto the nanotubes. From the fit, it was derived that $[Ce]_{c,m}$ was 10 mg/g, value which coincided with the experimental one, whereas k was of 0.15 g/L. From the next expression:

$$R_L = \frac{1}{1+k[Ce]_{aq,0}} \tag{7}$$

it was estimated that R_L<1, indicating that metal uptake is as favourable process for all the cerium concentrations used in this work [37].

3.1.4. Effect of the dosage absorbent on cerium adsorption

In Table 4, the obtained percentage of cerium adsorption at various MWCNTs dosages were given.

Table 4. Cerium adsorption versus MWCNTs dosage.

Nanotubes dosage, g/L	% Ce(III) adsorption
1	0.5
2	28
3	99
4	99

Aqueous solution: 0.01 g/L Ce(III) at pH 6. Temperature: 25º C. Time: 5 h. Stirring speed: 500 min^{-1}

Results obtained revealed that there was an increase in the percentage of cerium adsorption with the increase of the adsorbent dosage up to 3 g/L, and then no significant change in this percentage at higher adsorbent dosage.

3.2. Adsorption using oxidized multiwalled carbon nanotubes (ox-MWCNTs)

Having this adsorbent carboxylic acid as functional groups, it is logical to attribute metal uptake onto the adsorbent to the next equilibrium:

$$3(R-COOH)_c + Ce^{3+}_{aq} \leftrightarrow (R-COO^-)_3Ce^{3+}_c + 3H^+_{aq} \tag{8}$$

in the above equation, c and aq represented the carbon and aqueous phases, respectively, and R to the nanotubes matrix. Accordingly, cerium uptake by these adsorbents is attributed to a cation exchange process, in which the metal uptake onto the nanotubes is accompanied by the release of protons to the aqueous solution.

3.2.1. Influence of the stirring speed

Experiments were carried out to establish the adequate hydrodynamic conditions to the system. Results obtained are shown in Fig. 1. Near constant adsorption for stirring speeds in the 500-1000 min^{-1} was obtained, thus, the thickness of the aqueous diffusion layer and the aqueous resistance to mass transfer were minimized.

Peer-reviewed version available at Metals 2020, 10, 1057; doi:10.3390/met10081057

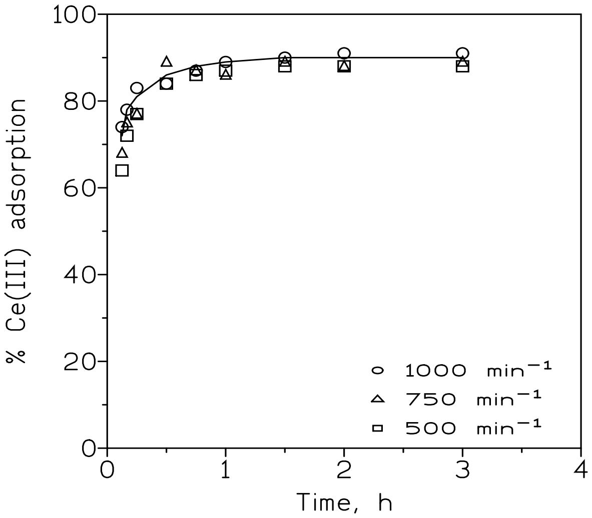

Figure 1. Influence of the stirring speed on the adsorption of cerium(III). Aqueous phase: 0.01 g/L Ce(III) at pH 6. ox-MWCNTs dosage: 1 g/L. Temperature: 25º C.

Experimental results were used to estimate the kinetics model which fitted to these values. These calculations showed that the pseudo-second order kinetic model (eq. (3)) best fitted ($r^2 = 1.0$) to the experimental results; from this fit, the equilibrium cerium concentration in the carbon material was of 9 mg/g (value which fitted perfectly with the experimental one), whereas the rate constant for the model was of 100 g/mg.min.

3.2.2. Influence of the initial cerium concentration

A series of tests was performed using aqueous solutions with different contents of cerium at pH 6. The adsorbent dosage was of 0.5 g/L.

Table 5 shows the variation of cerium adsorption and metal uptake onto the adsorbent for the different metal concentrations. These show that the increase of the initial cerium concentration tends to decrease the percentage of metal adsorption.

Table 5. Influence of initial cerium concentration in metal adsorption.

$[Ce]_{aq,0}$, g/L	% Ce(III) adsorption
0.01	92
0.02	92
0.03	77
0.04	61
0.06	39
0.08	30

Temperature: 25º C. Time: 5 h. Stirring speed: 500 min-1

Different isotherm models were used to estimate their fit to the experimental values derived from the data showed above. The results from this fit indicated that the cerium uptake was best represented (r^2= 0.9997) by the Langmuir Type-1 isotherm (eq. (6)), resulting in a k values of 3 L/mg

Peer-reviewed version available at Metals 2020, 10, 1057; doi:10.3390/met10081057

and $[Ce]_{c,m}$ of 48 mg/g, result which coincides with the experimentally finding value. By the use of eq. (7), it was found that $R_L<1$, indicative of a favourable exchange process.

3.2.2. Influence of the pH

The variation in the adsorption, as a function of the aqueous pH value, at 0.5 g/L carbon nanotubes dosage, has been investigated. The experimental conditions were: aqueous phases containing 0.01 g/L Ce(III) at various pH values, Temperature 25º C, time 5 h and stirring speed of 500 min^{-1}.

Results are shown in Figure 2, in which a decrease in cerium adsorption occurs as the pH of the solution decreases. The results can be explained according which it is shown in eq. (8), that is, a shift of the equilibrium to the left as the proton concentration in the solution increases.

From this eq. (8):

$$\boldsymbol{K} = \frac{[\boldsymbol{Ce}]_c[\boldsymbol{H}^+]^3_{aq}}{[\boldsymbol{ox-MWCNTs}]_c[\boldsymbol{Ce}^{3+}]_{aq}} \tag{8}$$

and:

$$\log D = \log C + 3\,pH \tag{9}$$

considering:

$$D = \frac{[Ce]_c}{[Ce^{3+}]_{aq}} \tag{10}$$

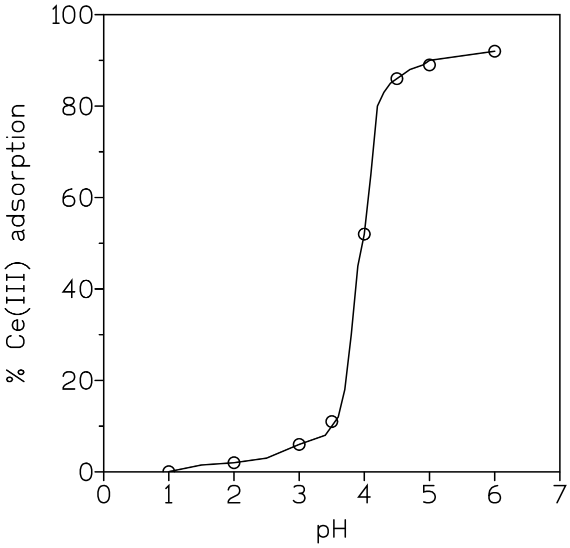

Figure 2. Plot of % Ce(III) adsorption versus pH.

In the above equation (10), the subscripts c and aq denote the carbon and aqueous phases, and the term log C represented the other terms as in eq. (8). Thus, and from eq. (9), a plot of log D versus pH may result in a line with slope 3; from results presented in Fig.3, such plot has effectively a slope near 3.

Peer-reviewed version available at Metals 2020, 10, 1057; doi:10.3390/met10081057

The results at pH 6 are used to estimate the rate law governing the adsorption of cerium onto the nanotubes.

3.2.3. Influence of the of the adsorbent dosage on adsorption of cerium

The results concerning adsorption of cerium(III) from an aqueous solution containing 0.01 g/L Ce(III) at pH 6, and varying dosages of the adsorbent in the range 0.13-1 g/L, revealed no change in the percentage of cerium adsorption (92%) at higher adsorbent dosages (0.5-1 g/L) against the values of 31% and 60% yielded at dosages of 0.13 and 0.25 g/L, respectively. In these series of experiments, other experimental variables were fixed as in Table 5.

3.3. Desorption

As it is shown in previous subsections, the pH of the aqueous solution has a great influence on cerium(III) adsorption, thus, the desorption step was investigated by the use of acidic solutions as desorbents on both nanomaterials. The experiments are carried out, at 25º C, using 0.1 M H2SO4 solutions, and a Ce-loaded carbon nanomaterial in a 0.4 carbon/solution relationship. From these experiments, it is shown that the percentage of cerium desorption is 75% and 84% in the case of the non-oxidized and the oxidized nanomaterials, respectively. Together to the recovery of the metal, the carbon nanotubes are recovered for further use; in the case of the non-oxidized MWCNTs, the use of non-concentrated acidic solution activates the adsorption sites present in the nanomaterial matrix, without destroying it, however, and as it is shown in the literature38, different behaviour between initial and eluted carbon material might be observed under continuous use, i.e. columns. In the case of the oxidized nanotubes, this regeneration is caused by shifting to the left the equilibrium, showed in eq. (8), as a consequence of the desorption reaction.

With respect to the above results, the use of HCl or HNO_3 solutions, as desorbents, do not improve the respective percentages of cerium desorption.

4. Conclusions

Experimental results showed that it is possible to use both commercial available nanomaterials to adsorb Ce(III) from aqueous solutions.

For both nanomaterials, the adsorption of cerium, is influence by a number of variables, including, metal concentration, adsorbent dosage, and the pH of the aqueous solution. However, the stirring speed applied on the system has near a negligible influence on cerium uptake.

Using both adsorbents, the metal uptake responded to the pseudo-second order kinetic model and the Langmuir Type-1 isotherm model, however, they differ in the rate law, as the film diffusion model fitted the uptake when the non-oxidized material is used, against the fitting of the particle diffusion model to the results yielded when the oxidized carbon nanotubes are used to remove cerium from the solution. The mechanism from which cerium is removed from the solution, using both nanomaterials, also appeared to be different: an adsorption process in the case of the non-oxidized nanomaterial against a cation exchange process in the case of the oxidized material. This is somewhat reflected in the fact that to obtain the same degree of cerium removal from the solution (more than 90%), the material dosage using the oxidized material is three times lower than that of the non-oxidized carbon nanotubes. Cerium loaded onto both nanomaterials can be desorbed by the use of sulphuric acid solutions.

Author Contributions: Conceptualization, F.J.A. and F.A.L.; methodology, F.J.A. and F.A.L.; formal analysis, I.G-D. and F.J.A.; investigation, F.J.A., F.A.L., I.G-D., E.E.B. and O.R.L.; resources, F.A.L.; writing—original draft

Peer-reviewed version available at *Metals* **2020**, *10*, 1057; doi:10.3390/met10081057

preparation, F.J.A.; writing—review and editing, F.J.A., F.A.L., I.G-D., E.E.B. and O.R.L. All authors have read and agreed to the published version of the manuscript

Funding: This research has received funding from the European Union's Horizon 2020 research and innovation program under grant agreement No 776851 (CarEService).

Conflicts of Interest: The authors declare no conflict of interest.

References

1. Alguacil, F.J.; Alcaraz, L.; García-Díaz, I.; López, F.A. Removal of Pb2+ in Wastewater via Adsorption onto an Activated Carbon Produced from Winemaking Waste. *Metals (Basel).* **2018**, *8*, 697.
2. Ihsanullah; Abbas, A.; Al-Amer, A.M.; Laoui, T.; Al-Marri, M.J.; Nasser, M.S.; Khraisheh, M.; Atieh, M.A. Heavy metal removal from aqueous solution by advanced carbon nanotubes: Critical review of adsorption applications. *Sep. Purif. Technol.* **2016**, *157*, 141–161.
3. Hu, Y.; Florek, J.; Larivière, D.; Fontaine, F.-G.; Kleitz, F. Recent Advances in the Separation of Rare Earth Elements Using Mesoporous Hybrid Materials. *Chem. Rec.* **2018**, *18*, 1261–1276.
4. Alguacil, F.J.; Garcia-Diaz, I.; Lopez, F.; Rodriguez, O. Removal of Cr(VI) and Au(III) from aqueous streams by the use of carbon nanoadsorption technology. *Desalin. Water Treat.* **2017**, *63*, 351–356.
5. García-Díaz, I.; López, F.A.; Alguacil, F.J. Carbon Nanofibers: A New Adsorbent for Copper Removal from Wastewater. *Metals (Basel).* **2018**, *8*, 914.
6. Egbosiuba, T.C.; Abdulkareem, A.S.; Kovo, A.S.; Afolabi, E.A.; Tijani, J.O.; Roos, W.D. Enhanced adsorption of As(V) and Mn(VII) from industrial wastewater using multi-walled carbon nanotubes and carboxylated multi-walled carbon nanotubes. *Chemosphere* **2020**, *254*, 126780.
7. Roccaro, P.; Sgroi, M.; Vagliasindi, F.G.A. Removal of Xenobiotic Compounds from Wastewater for Environment Protection: Treatment Processes and Costs. *Chem. Eng. Trans.* **2013**, *32*, 505-510 SE-Research Articles.
8. Guo, L.; Liu, Y.; Dou, J.; Huang, Q.; Lei, Y.; Chen, J.; Wen, Y.; Li, Y.; Zhang, X.; Wei, Y. Highly efficient removal of Eu3+ ions using carbon nanotubes-based polymer composites synthesized from the combination of Diels-Alder and multicomponent reactions. *J. Mol. Liq.* **2020**, *308*, 112964.
9. Ramasamy, D.L.; Puhakka, V.; Doshi, B.; Iftekhar, S.; Sillanpää, M. Fabrication of carbon nanotubes reinforced silica composites with improved rare earth elements adsorption performance. *Chem. Eng. J.* **2019**, *365*, 291–304.
10. Gambogi, J. *Rare Earths. Mineral commodity summaries 2020*; Reston, VA, 2020;
11. Omodara, L.; Pitkäaho, S.; Turpeinen, E.-M.; Saavalainen, P.; Oravisjärvi, K.; Keiski, R.L. Recycling and substitution of light rare earth elements, cerium, lanthanum, neodymium, and praseodymium from end-of-life applications - A review. *J. Clean. Prod.* **2019**, *236*, 117573.
12. Jowitt, S.M.; Werner, T.T.; Weng, Z.; Mudd, G.M. Recycling of the rare earth elements. *Curr. Opin. Green Sustain. Chem.* **2018**, *13*, 1–7.
13. Gao, J.; Si, Z.; Xu, Y.; Liu, L.; Zhang, Y.; Wu, X.; Ran, R.; Weng, D. Pd–Ag@CeO2 Catalyst of Core–Shell Structure for Low Temperature Oxidation of Toluene Under Visible Light Irradiation. *J. Phys. Chem. C* **2019**, *123*, 1761–1769.
14. Liu, X.; Zhang, T.C.; He, H.; Ouyang, L.; Yuan, S. A stearic Acid/CeO2 bilayer coating on AZ31B magnesium alloy with superhydrophobic and self-cleaning properties for corrosion inhibition. *J. Alloys Compd.* **2020**, *834*, 155210.
15. Nurhasanah, I.; Kadarisman; Gunawan, V.; Sutanto, H. Cerium oxide nanoparticles application for rapid

Peer-reviewed version available at *Metals* **2020**, *10*, 1057; doi:10.3390/met10081057

adsorptive removal of tetracycline in water. *J. Environ. Chem. Eng.* **2020**, *8*, 103613.

16. Rivoira, L.P.; Valles, V.A.; Martínez, M.L.; Sa-ngasaeng, Y.; Jongpatiwut, S.; Beltramone, A.R. Catalytic oxidation of sulfur compounds over Ce-SBA-15 and Ce-Zr-SBA-15. *Catal. Today* **2019**, *in press*.
17. Jacinto, J.; Henriques, B.; Duarte, A.C.; Vale, C.; Pereira, E. Removal and recovery of Critical Rare Elements from contaminated waters by living Gracilaria gracilis. *J. Hazard. Mater.* **2018**, *344*, 531–538.
18. Pujar, M.S.; Hunagund, S.M.; Barretto, D.A.; Desai, V.R.; Patil, S.; Vootla, S.K.; Sidarai, A.H. Synthesis of cerium-oxide NPs and their surface morphology effect on biological activities. *Bull. Mater. Sci.* **2019**, *43*, 24.
19. Wang, Y.; Xie, X.; Chen, X.; Huang, C.; Yang, S. Biochar-loaded Ce3+-enriched ultra-fine ceria nanoparticles for phosphate adsorption. *J. Hazard. Mater.* **2020**, *396*, 122626.
20. Shi, Y.; Zhao, Y.; Cao, M.; Chen, H.; Hu, Z.; Chen, X.; Zhang, Z.; Liu, Q. Dense Ce3+ doped Lu3A15O12 ceramic scintillators with low sintering adds: Doping content effect, luminescence characterization and proton irradiation hardness. *J. Lumin.* **2020**, *225*, 117336.
21. Silva, V.D.; Ferreira, L.S.; Araújo, A.J.M.; Simões, T.A.; Grilo, J.P.F.; Tahir, M.; Medeiros, E.S.; Macedo, D.A. Ni and Ce oxide-based hollow fibers as battery-like electrodes. *J. Alloys Compd.* **2020**, *830*, 154633.
22. Duan, J.; Tang, W.; Wang, R.; Tang, X.; Li, J.; Tang, M.; Li, P. Inhibited voltage decay and enhanced electrochemical performance of the Li-rich layered Li1.2Mn0.54Ni0.13Co0.13O2 cathode material by CeAlOδ surface coating modification. *Appl. Surf. Sci.* **2020**, *521*, 146504.
23. Liu, Y.; Yang, Z.; Li, J.; Niu, B.; Yang, K.; Kang, F. A novel surface-heterostructured Li1.2Mn0.54Ni0.13Co0.13O2@Ce0.8Sn0.2O2−σ cathode material for Li-ion batteries with improved initial irreversible capacity loss. *J. Mater. Chem. A* **2018**, *6*, 13883–13893.
24. EU Report on critical raw materials and the circular economy - Publications Office of the EU Available online: https://publications.europa.eu/en/publication-detail/-/publication/d1be1b43-e18f-11e8-b690-01aa75ed71a1/language-en/format-PDF/source-80004733 (accessed on Feb 18, 2019).
25. Parisi, F. Adsorption and Separation of Crystal Violet, Cerium(III) and Lead(II) by Means of a Multi-Step Strategy Based on K10-Montmorillonite. *Minerals* **2020**, *10*, 466.
26. Han, Q.; Du, M.; Guan, Y.; Luo, G.; Zhang, Z.; Li, T.; Ji, Y. Removal of simulated radioactive cerium (III) based on innovative magnetic trioctylamine-polystyrene composite microspheres. *Chem. Phys. Lett.* **2020**, *741*, 137092.
27. Wójcik, G. Sorption Behaviors of Light Lanthanides(III) (La(III), Ce(III), Pr(III), Nd(III)) and Cr(III) Using Nitrolite. *Materials (Basel).* **2020**, *13*, 2256.
28. Jiménez-Reyes, M.; Almazán-Sánchez, P.T.; Solache-Ríos, M. Behaviour of cerium(III) in the presence of components of soils and its humate complex. *Environ. Technol.* **2020**, *in press*, 1–9.
29. Parisi, F.; Lazzara, G.; Merli, M.; Milioto, S.; Princivalle, F.; Sciascia, L. Simultaneous Removal and Recovery of Metal Ions and Dyes from Wastewater through Montmorillonite Clay Mineral. *Nanomaterials* **2019**, *9*, 1699.
30. Zhao, L.; Azhar, M.R.; Li, X.; Duan, X.; Sun, H.; Wang, S.; Fang, X. Adsorption of cerium (III) by HKUST-1 metal-organic framework from aqueous solution. *J. Colloid Interface Sci.* **2019**, *542*, 421–428.
31. Bouchmila, I.; Bejaoui Kefi, B.; Souissi, R.; Abdellaoui, M. Purification, characterization and application of cherty rocks as sorbent for separation and preconcentration of rare earths. *J. Mater. Res. Technol.* **2019**, *8*, 2910–2923.
32. Kołodyńska, D.; Hubicki, Z.; Fila, D. Recovery of rare earth elements from acidic solutions using macroporous ion exchangers. *Sep. Sci. Technol.* **2019**, *54*, 2059–2076.
33. Fila, D.; Hubicki, Z.; Kołodyńska, D. Recovery of metals from waste nickel-metal hydride batteries using

multifunctional Diphonix resin. *Adsorption* **2019**, *25*, 367–382.

34. Alguacil, F.J.; Lopez, F.A.; Rodriguez, O.; Martinez-Ramirez, S.; Garcia-Diaz, I. Sorption of indium (III) onto carbon nanotubes. *Ecotoxicol. Environ. Saf.* **2016**, *130*, 81–86.
35. Bayazit G., T.B.E. and G.Ü.D. Biosorption, isotherm and kinetic properties of common textile dye by Phormidium animale. *Glob. NEST J.* **2020**, *22*, 1–7.
36. Hubbe, M. A., Azizian, S., and Douven, S. Implications of apparent pseudo-second-order adsorption kinetics onto cellulosic materials: A review. *BioResources* **2019**, *14*, 7582–7626.
37. Foo, K.Y.; Hameed, B.H. Insights into the modeling of adsorption isotherm systems. *Chem. Eng. J.* **2010**, *156*, 2–10.